IEEE Open Access Journal of
Power and Energy

Received 16 April 2024; revised 25 June 2024; accepted 28 June 2024.
Date of publication 10 July 2024; date of current version 19 July 2024.

Digital Object Identifier 10.1109/OAJPE.2024.3425893

Switching Analysis in Hybrid OHL-Submarine Cable 500-kV Transmission System

BINHOT P. NABABAN[1,2], KEVIN MAROJAHAN BANJAR-NAHOR[1] (Member, IEEE), MUSA PARTAHI MARBUN[3] (Member, IEEE), SUWARNO[1] (Senior Member, IEEE), AND NANANG HARIYANTO[1] (Member, IEEE)

[1]School of Electrical Engineering and Informatics, Institut Teknologi Bandung, Bandung 40132, Indonesia
[2]PLN Enjiniring, Jakarta 11420, Indonesia
[3]System Planning Division, PLN, Jakarta 12160, Indonesia
CORRESPONDING AUTHOR: B. P. NABABAN (binhot.nababan@gmail.com)

ABSTRACT This study focuses on analyzing switching transients in the upcoming 500 kV Java-Bali Connection (JBC) hybrid OHL and submarine cable project using DIgSILENT PowerFactory software, based on a realistic power system model. Distributed-parameter models with constant parameters of the Bergeron model are utilized. Analysis of the traveling wave effect on the line is conducted, and the integration time step based on the time of the traveling wave is carefully selected. Statistical distributions of energization are produced by varying the circuit configuration and system short-circuit power. It is found that the Switching Withstand Voltage (SWV) during the energization process remain below 1175 kV. The probability distribution is fitted to a normal distribution, with the skewness and kurtosis shown to be skewed to the right and having a lower peak than that of the normal distribution, respectively. When a three-phase short-circuit at the line breaker is induced, the rate of rise of recovery voltage (RRRV) exceeds the IEC standard envelope if only one circuit is operating. In this contribution, switching analysis during no-load energization and de-energization in the planning stage of the mixed OHL-submarine cable is examined.

INDEX TERMS Line de-energization, line energization, statistical distribution, submarine cable, transient overvoltages, TRV.

I. INTRODUCTION

EXTRA high voltage (EHV) power transmission grids play a vital role in facilitating the transfer of substantial quantities of electric power from generation facilities to consumption sites. As per the IEC 60038 [1], EHV is classified as voltage exceeding 245 kV. The Java-Bali system, recognized as Indonesia's largest power grid system, operates with a backbone categorized as EHV, using a 500 kV system. The Java-Bali Connection (JBC) 500 kV transmission line is expected as one of the priority projects in Java-Bali system. The planning of JBC extends from the existing Paiton substation to the planned Antosari substation, encompassing total an overhead lines (OHL) section of 267.9 km and a submarine cable section of 6.5 km [2]. The JBC represents the first, the highest voltage level, and the longest length implementation project of EHV submarine cables in Indonesia.

Self-contained fluid-filled (SCFF) and cross-linked polyethylene (XLPE) are the two technologies that can be employed for high-power submarine cable application [3]. XLPE technology, which boasts excellent physical and chemical attributes, superior insulation capabilities, and straightforward manufacturing and installation, is currently preferred for ensuring a secure and reliable power supply [4]. However, there have been only few high-power submarine cable projects that have utilized XLPE technology to date. The Zoushan project, located in China, became the world's first to use a 500 kV XLPE submarine cable, spanning 15.5 km, and operation was initiated in 2019 [5], [6], [7].

This research focuses on the phenomena related to transients caused by the switching process of hybrid OHL-submarine cables in the JBC project. The switching events under investigation are line energization and de-energization. The reliable model of the Java-Bali interconnection system is primarily used as base model and the simulation results are assessed according to relevant IEC and grid code requirements. Electromagnetic phenomena are

analyzed using an electromagnetic transient (EMT) feature in the DIgSILENT PowerFactory program. This program takes into account detailed aspects such as unbalanced operating conditions, the coupling effect, distributed parameters of lines, equipment saturation, etc. Frequency-dependent models for electrical components must be integrated into power systems for EMT simulations.

EMT simulation uses differential equations to represent voltage and current [8]. To solve these differential equations, a numerical technique is utilized to simulate the response of the system. This technique requires solving the problem at regular intervals, called integration time steps. For switching transients, the integration time step must be smaller than the minimum travel time of the propagation wave, with half of this travel time being recommended [9]. The time scale for travelling time can reach microseconds. Therefore, this necessitates smaller time steps, which in turn result in greater computational expenses. Hence, it becomes essential to simplify the network system to reduce computational effort [10].

The evaluation of switching transients are very critical in EHV range. Hence, switching analysis is mandatorily required. A detailed statistical distribution, as a basis for insulation coordination, is performed to assess the overvoltages under different operational conditions of the circuit lines and varying short-circuit power due to the decommissioning of certain generator units. For de-energization transients, the study investigates the transient recovery voltage (TRV) across circuit-breaker (CB) contacts during line de-energization and examines the line CB capability in the event of terminal faults.

II. THEORETICAL BACKGROUND

Abnormal patterns of current and voltage with larger amplitude than the steady state and with limited duration are known as transients. Voltage level, system topology, and short circuit power are parameters that influence transients [11]. In electrical power systems, transients are described in terms of electromagnetic fields and travelling waves. In terms of frequency range, line switching and fault clearing are categorized as slow-front surges (from 50 Hz to 20 kHz). Due to the involvement of high frequencies, the representation of OHL and cables using lumped elements cannot be used. Instead, elements of capacitance and inductance, which are uniformly distributed, should be utilized [12].

As a consequence of structural differences between OHL and cable, the series inductance per unit length of a cable can be reduced by up to five times, the shunt capacitance to earth can increase by up to twenty times, the surge impedance can be reduced by roughly tenfold, and the traveling wave velocity is approximately half that of overhead lines [13]. The mismatch in frequency-dependent characteristic impedance causes complex electromagnetic wave propagation, as some waves will be transmitted or reflected, resulting in a traveling wave that has the potential to cause overvoltage [14], [15].

Reactive power produced by the line is directly proportional to its voltage and geometry. If there is an excess of reactive power under certain operating conditions, causing the power-frequency voltage to rise above the limits set by the grid code, the use of reactive power compensation equipment becomes essential. The commonly used equipment for this purpose is a line-connected shunt reactor (SR). However, there could be the potential for parallel resonance in a double circuit compensated with an SR. Parallel resonance occurs due to capacitive coupling between the circuits. The degree of compensation provided by reactor determines the severity of the resonance [16], [17].

A short circuit occurring directly at the terminals of a CB is known as a terminal fault. This type of fault is extremely rare but represents the highest fault current that the CB may encounter. After the natural current zero crossing, the fault is cleared, and TRV emerges. TRV in a CB appears as a voltage difference between the two sides of the contacts (phase to earth). The fault has an inductive characteristic and current lags the voltage by almost 90°. Thus, when zero current is crossing, voltage is at the peak. This causes the TRV to reach maximum value, because TRV components are superimposed on the peak value of power-frequency component.

The TRV associated with faults is characterized by the rate-of-rise of recovery voltage (RRRV) and the TRV peak. RRRV is crucial due to the thermal stress caused by the arc before current zero, and the TRV peak voltage causes electrical stress to the dielectric components [18]. In the case of a terminal fault, the RRRV is the highest, while the voltage for the first TRV peak is relatively lower. SF_6 CBs face a significant challenge with the steep rise of RRRV, whereas the first peak of TRV parameter does not have as much impact [11]. The TRV wave generally depends on the earthing system, network configuration, location of the fault, etc.

III. PROJECT DESCRIPTION AND SYSTEM MODELLING

A. JBC PROJECT

The plan for the JBC project is illustrated in Fig. 1. While Paiton substation is an existing facility, Kalipuro substation and Antosari substation are planned to be constructed. The transmission from Paiton substation to Kalipuro substation employs 4 x Zebra two-circuit conductors with an estimated line length of 181 km. Single towers capable of accommodating two circuits are used. From the Kalipuro substation to the Banyuwangi landing point, an overhead line with a length of 4.8 km, having specifications similar to those from the Paiton substation to the Kalipuro substation, is utilized.

The submarine cable, with a cross-sectional area of 1600 mm^2, single-core XLPE technology, connects the Banyuwangi landing point to the Gilimanuk landing point. The landing point serves as a transition facility from OHL to submarine cables. From the Gilimanuk landing point to Antosari substation, an OHL with 4 x Zebra two-circuit conductors is employed, with an estimated line length of 82.1 km. The cross-section of Zebra conductor is 450 mm^2, with 54 aluminum wires and 7 steel wires [19].

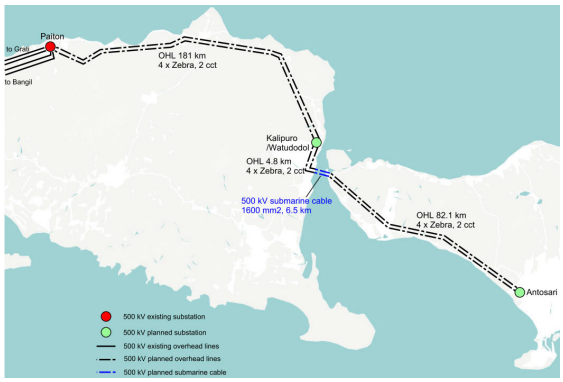

FIGURE 1. **JBC project map.**

B. SYSTEM MODELLING

For the EMT simulation, the detailed model of the system generally must extend to at least two buses away from the point of interest (Fig. 2) [20]. The line under examination in this investigation is the one linking the Kalipuro substation to the Antosari substation.

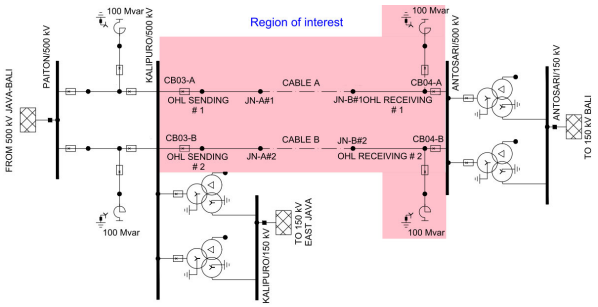

FIGURE 2. **System configuration for EMT simulation.**

An SR with a capacity 100 MVAr per circuit is installed to limit the steady-state overvoltages after switching process especially at the receiving end due to the Ferranti effect. These devices are installed at the Kalipuro and Antosari substations. The SR is equipped with a dedicated CB to enhance switching flexibility. Neutral reactor is installed at neutral point of SR to reduce the secondary arc current. The neutral reactor is rated at 562 kVar, with a reactance of 2471 Ω and a resistance of 23.3 Ω.

The model does not include surge arresters to simulate the most severe overvoltages. However, a surge arrester is a mandatory component that must be installed at the line terminal. The arrester design is a gapless zinc oxide (ZnO) type. The switching impulse protective data with current wave of 30/60 μs of the surge arrester is presented in Table 1.

C. STEADY-STATE SIMULATION

Steady-state simulations utilize the representation of the entire Java-Bali 500 kV and 150 kV power system within the DIgSILENT PowerFactory environment. Through this approach, realistic load-flow and short-circuit simulations can be simulated based on the anticipated operational date

TABLE 1. **Switching impulse protective data for surge arrester.**

Current (kA_{peak})	Voltage (kV_{peak})
0.5 kA	795
1.0 kA	816
2.0 kA	844

of the JBC project in 2026 [21]. The simulations, conducted under low load conditions, aim to highlight the most severe switching overvoltages [22], [23].

It is not possible to conduct detailed modeling of all relevant parts of the Java-Bali transmission system for EMT simulation. Therefore, network reduction is required. Within PowerFactory, the external grid element (*RlmXnet*) is used to represent external networks, and it will be applied at the 500 kV Paiton substation, the 150 kV Kalipuro substation, and the 150 kV Antosari substation. Separate load flow and short-circuit simulations are conducted. The results of these simulations are used as input data in the external grid (Table 2).

TABLE 2. **Input for external grid from load flow simulation.**

External network location	Bus type	Active power (MW)	Reactive power (MVAr)	Voltage set point (pu)
500 kV Paiton	Slack bus	-	-	1.028
150 kV Kalipuro	PQ bus	-217.2	-5.2	-
150 kV Antosari	PQ bus	-237.6	71.2	-

For the PQ bus type, the external grid is modeled as a constant P (active power) and constant Q (reactive power) infeed, where positive P values indicate generated active power (as a generator) and negative values indicate consumed active power (as a load), with similar considerations for reactive power. Thus, at the 150 kV Kalipuro bus, 217.2 MW of active power and 5.2 MVAr of reactive power are absorbed (flowing downstream to 150 kV system), while at the 150 kV Antosari bus, 237.6 MW of active power is absorbed (flowing downstream to 150 kV system), and 71.2 MVAr of reactive power is supplied (flowing upstrem to 500 kV system). As for the slack bus type, the voltage set point (in per unit) must be defined by the user [24]. The voltage set point for the slack bus in the 500 kV Paiton substation is 1.028 pu, determined from load flow simulation for the entire Java-Bali power grid.

The input data for the external grid from short-circuit simulation is displayed in Table 3. Obtaining these figures involves performing a phase-to-ground short-circuit fault at the points representing the bus bars where the external network will be connected.

The method employed is IEC 60909 with a voltage c factor value of 1.1. X/R represents the peak ratio of positive sequence reactance to resistance, X_0 denotes the imaginary

TABLE 3. Input for external grid from short circuit simulation.

External network location	SC power (MVA)	R/X	X_0/X_1	R_0/X_0
500 kV Paiton	12727	0.057	0.324	0.018
150 kV Kalipuro	1367.5	0.176	0.104	0.010
150 kV Antosari	1108.9	0.148	0.084	0.011

part of the zero-sequence impedance, and R_0 signifies the real part of the zero-sequence impedance.

The line charging for OHL is approximately 1.1 to 1.2 MVAr/km, while for submarine cables, it ranges from 15.6 to 16.1 MVAr/km, depending on the number of circuits operated. Reactor compensation level is estimated by comparing reactor MVAr capacity to the MVAr of line. Consequently, the compensation level of reactor to the line is approximately 49%.

D. MODELLING OF TRANSMISSION LINES

Transients in power systems are responsible for generating travelling electromagnetic waves with high-frequency range. In this frequency range, it is necessary to represent the distributed combination of the capacitance, inductance, and frequency-dependent resistance [25].

Conservative outcomes produced by Bergeron models lead to their frequent selection due to their numerical stability and reduced computational requirements. When findings exceed the equipment's withstand voltages or other specified ratings, detailed investigations are initiated using frequency-dependent models, which are valued for their greater precision [13]. The constant parameter model from DIgSILENT PowerFactory, which is based on the Bergeron theory, is utilized for representing OHL and XLPE cables in the developed EMT model for the JBC project.

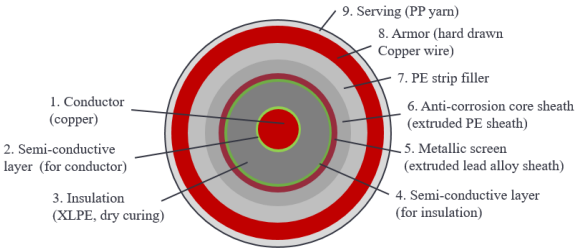

FIGURE 3. The construction and layers of XLPE submarine cable.

Single-core marine cable with a metal sheath around the core and conductive armoring is employed. The basic construction of a typical XLPE cable is shown in Fig. 3. The geometry and material characteristics utilized as input parameters for the cables of the JBC in DIgSILENT PowerFactory are presented in Table 4.

TABLE 4. Thickness and material properties to model submarine cable.

Layer	Thickness (mm)	Relative Permittivity
Conductor	23.8	-
Semi-conductive layer (outer core)	2.3	-
Insulation	32	2.5
Semi-conductive layer (outer insulation)	1.5	-
Metallic screen (extruded lead alloy sheath)	5	-
Anti-corrosion core sheath (extruded PE sheath)	10	2.3
Armor (hard drawn Copper wire)	6	-
Serving (PP yarn)	7	2.8

The cable consists of a single-core 1600 mm^2 copper conductor cable with a DC-resistance at 20 °C is 0.0113 Ω/km and a characteristic impedance 37 Ω.

The cross-sectional layout of the cable circuits (Fig. 4) is characterized by a flat formation within an open cable trench. The distance between phases, set at 0.45 m according to the feasibility study document for the JBC project, conforms to the detailed installation requirements outlined for each cable [26]. However, the distance between circuits is not clearly identified in the feasibility study document. It is common practice to install a group of single-core cables with a certain distance between them, typically up to several hundred meters, to avoid multiple damages [3]. In this study, a distance of 50 m between circuits is taken into account, based on the 500 kV Zouhan project [4].

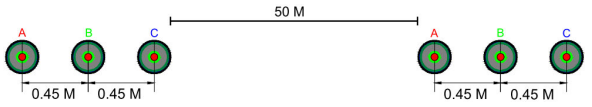

FIGURE 4. Cable cross-sectional with flat formation.

In this scenario, solid bonding is applied at both ends of the submarine cable [3], [27]. As a result, the reduced option method is adopted in the cable model, leading to a reduction in the dimensions of the impedance and admittance matrices, which in turn facilitates faster solution speeds with minimal impact on accuracy [28].

Lattice steel tower technology is utilized in the OHL, following the reference standard [29]. The conductor arrangement is vertical. The tower type is a single tower capable of accommodating two circuits. The geometry of the towers used is illustrated in Fig. 5. In high voltage transmission lines, bundle conductors are frequently used to minimize corona losses. A symmetrical bundle is formed by holding conductors with spacers. The spacing between bundle conductors is 0.45 m. Aluminum conductor steel-reinforced (ACSR) is used for the OHL conductors, which have a resistance of

0.0642 ohm/km, while aluminum-clad steel is used for the shield wire. Two shield wires are installed on each tower to provide protection against lightning strikes. The characteristic impedance of OHL is 258 Ω. In general, the specifications of the conductors and shield wires inputted into the simulator can be seen in Table 5.

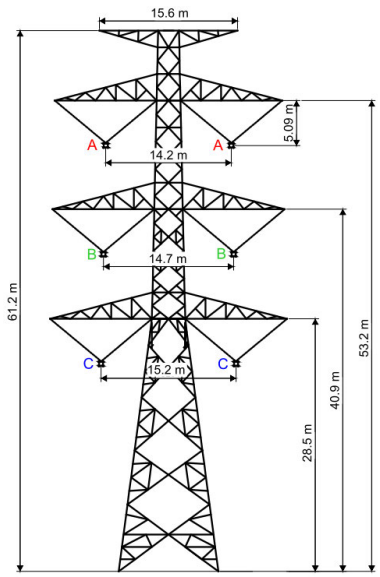

FIGURE 5. **OHL tower geometry.**

TABLE 5. **Conductor and shield wire properties.**

Parameter	Phase Conductor	Shielding Wire
Conductor	ACSR	Aluminum-clad steel (AS) wire
Stranding and wire diameter aluminum (no./mm)	54/3.21	-
Stranding and wire diameter steel (no./mm)	7/3.21	8/4.1
DC resistance at 20 °C (Ω/km)	0.0642	0.492
Relative permeability	1	1
Number of sub-conductors	4	-
Bundle spacing (m)	0.45	-
Sag (m)	18	-

IV. LINE ENERGIZATION IN HYBRID OHL-SUBMARINE CABLE

A. SIMULATION CONSIDERATION

The switching is performed from the Kalipuro substation while the circuit remains open on the other side. The calculated minimum travelling wave was 16 μs, so a simulation time step of 5 μs was selected for the transient studies to maintain a balance in simulation accuracy and time.

B. LINE ENERGIZATION OVERVOLTAGES

In this scenario, the simulation of energizing overvoltages involving untransposed lines was conducted. The initial energization of the line is by closing CB of SR followed by the closing of CB03-B (Fig. 6).

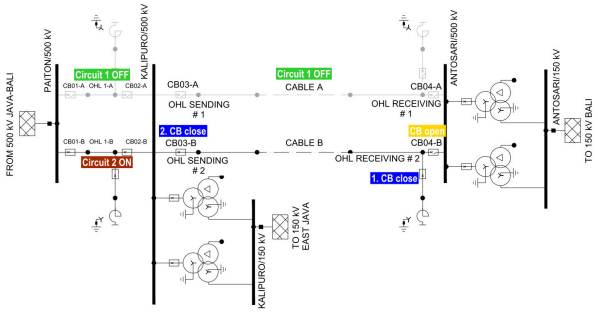

FIGURE 6. **The stages of line energization.**

It was assumed in these simulations that the closure of CB03-B occurred simultaneously at the peak voltage of phase B (t = 86.3 ms). The selection of phase B was conducted because that phase is having the highest voltage among the other phases at the Kalipuro substation before the energizing process is conducted. Fig. 7 is depicted the voltage of each phase at the Kalipuro substation subsequent to the energization of circuit 2. Phase voltage B is represented by the red graph. Switching occurs at the peak voltage, resulting in phase B being exhibited as having the highest voltage compared to the other phases.

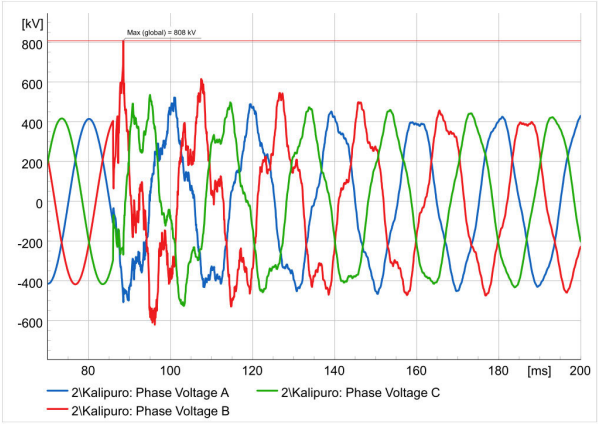

FIGURE 7. **Phase voltage at kalipuro substation after line energization.**

In Fig. 8, the energization voltage at the open-end is depicted, with overvoltage amplitude reach the highest at 938.8 kV (2.29 pu) observed in phase B due to the switching event is conducted at its maximum voltage. One can also notice that the highest value is typically reached at the receiving end. All the highest overvoltages are still below the switching withstand voltage (SWV) as recommended in [30], which is 1175 kV (peak value).

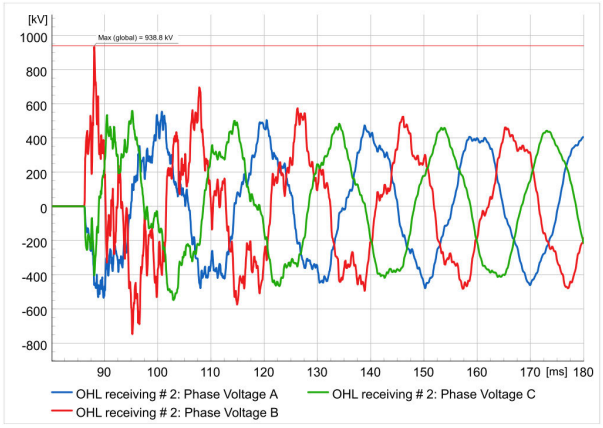

FIGURE 8. Phase voltage at antosari substation after line energization.

Fig. 9 shows the phase voltage demonstrating the travelling wave effect at the line terminal and the OHL-submarine cables joint of circuit 2. These cable joints are indicated as JN-A#2 and JN-B#2 (see Fig. 2). At the joint, a portion of the energy is transmitted through, and a portion is reflected back, calculated by equation (1) and (2).

$$V_R = \frac{Z_2 - Z_1}{Z_2 + Z_1}.V_I \tag{1}$$

$$V_T = \frac{2Z_2}{Z_2 + Z_1}.V_I \tag{2}$$

where V_R is reflected wave, V_T is transmitted wave, V_I is incident voltage wave, Z_1 is first transmission line surge impedance, and Z_2 is second transmission line surge impedance.

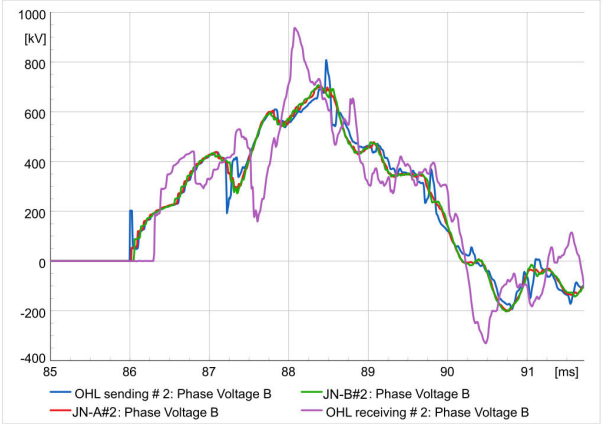

FIGURE 9. Phase voltage showing travelling wave.

Approximately 26% of the wave is transmitted and 74% is reflected for the case where the wave travels from the OHL to the submarine cable section. Similarly, for the case where the wave travels from the submarine cable to the OHL (from Gilimanuk landing point to Antosari substation), 174% of the wave is transmitted, and 74% is reflected. It is also evident that there is a delay effect at the observation point as a result of using a distributed line model.

C. THE EFFECT OF ELECTROMAGNETIC COUPLING IN DE-ENERGIZED LINE

This section examines the effects of power frequency voltage induced in the de-energized circuit through capacitive coupling with the live phase. The circuit 1 designated to be the disconnected circuit, while the circuit 2 stayed energized. Fig. 10 illustrates the condition where the ES in circuit 1 is open, representing the state where the off-line circuit is about to be energized. Fig. 11 reveals the emergence of voltage in circuit 1, where the peak voltage (phase A) measured at the sending end is 26 kV and at the receiving end is 27.46 kV.

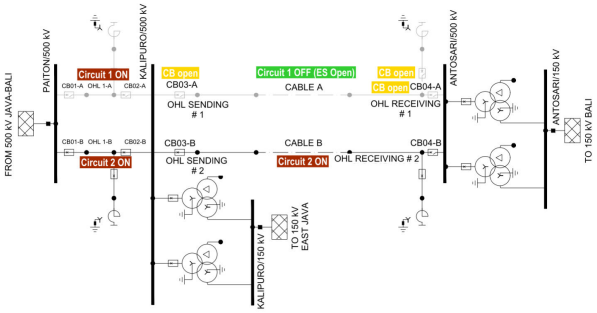

FIGURE 10. Configuration when ES open at circuit 1 of kalipuro - antosari line.

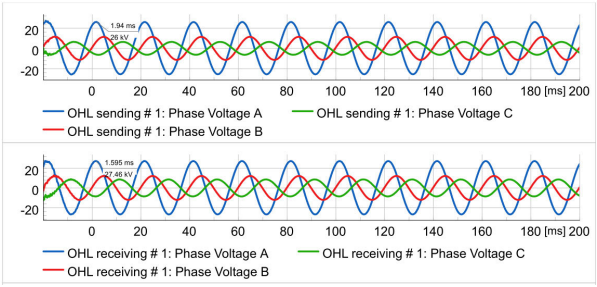

FIGURE 11. Induced voltage at circuit 1 when ES open.

The next step involves examining the impact of the SR insertion to determine if there is any potential danger of parallel resonance occurring due to the introduction of this reactor. Parallel resonance is induced by the interaction of line-connected SR with the remaining energized phase through capacitive coupling [17]. With the reactor inserted, the voltage at the receiving end on phase A is 59.33 kV (Fig. 12). Thus, at a reactor compensation level of 49%, potential temporary overvoltage problems caused by parallel resonance will not occur.

D. STATISTICAL ANALYSIS OF LINE OVERVOLTAGES

The statistical distribution of energization overvoltages is highly recommended for studying insulation coordination, given the stochastic nature of CB closing times [31]. Table 6

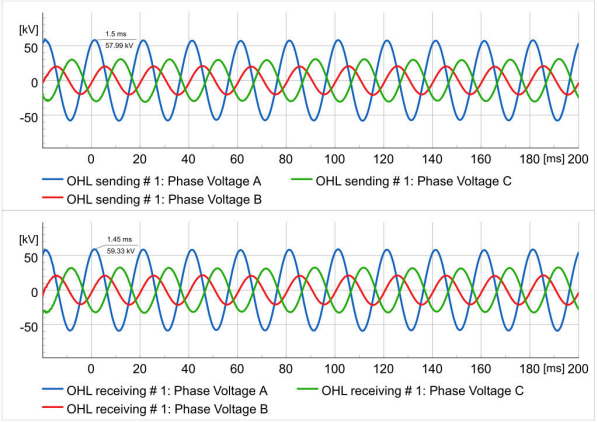

FIGURE 12. Induced voltage at circuit 1 when ES open and CB of reactor close.

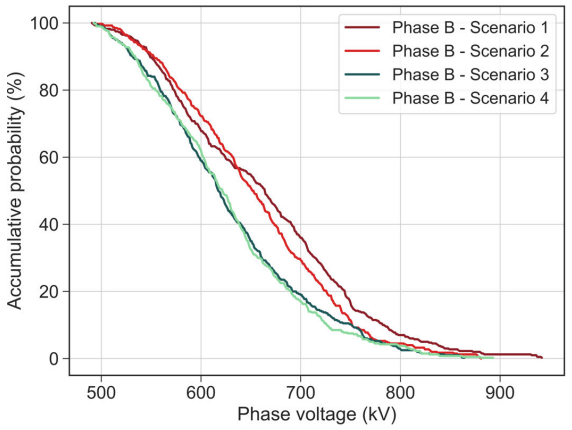

FIGURE 13. Accumulative probability distribution of overvoltages for combination of circuit state case.

shows input parameter for conducting statistical switching simulation.

TABLE 6. Input parameter for statistical switching simulation.

Description	Value
Maximum dispersion time for closing time	10 ms
Maximum scatter time for poles	3 ms
Number of runs	400
Report probability (%)	2%

The number of statistical switching case studies should be 100 or more [32]. The statistical calculation for energization overvoltages was carried out 200 times [33]. Furthermore, in [34], 400 energizations were conducted for each study case to increase the accuracy of the statistical distribution results. In this study, 400 simulations scenario are carried out to ensure accurate results.

1) IMPACT VARIATION OF LINE OPERATING CONFIGURATION

The combinations of ON and OFF states are depicted in Table 7. The point of interest is on the receiving side at phase B. The switching sequence starts with the closing of CB reactor, followed by the CB at the sending side. In Fig. 13, the cumulative probabilities of overvoltage energization are depicted. The probability of overvoltages exceeding the specified threshold is shown on the vertical axis, while the horizontal axis represents the overvoltage values.

Table 8 presents the maximum, mean, standard deviation, and 2% values. These are the four key values for evaluating the statistical distributions. The overvoltage level at which the probability of exceeding the value is 2% is defined as the 2% value. This parameter is used as the basis for insulation coordination studies.

Scenario 1 exhibits the highest overvoltage, while scenario 4 results in the lowest overvoltage. The 2% value for scenario 1 is 850.25 kV (2.08 pu), whereas for scenario 4 it is 784.13 kV (1.92 pu). This outcome is also illustrated in Fig. 13, where the highest probability of overvoltage is observed in Scenario 1.

TABLE 7. On-off combination of circuits.

Scenario	Paiton - Kalipuro		Kalipuro - Antosari	
	Cct 1	Cct 2	Cct 1	Cct 2
Scenario 1	OFF	ON	OFF	To be energized
Scenario 2	ON	ON	OFF	To be energized
Scenario 3	OFF	ON	ON	To be energized
Scenario 4	ON	ON	ON	To be energized

TABLE 8. Overvoltage distribution key parameters for variation of line operating configuration.

Scenario	Overvoltages (kV)			
	Max	Mean	Std dev	2% value
Scenario 1	941.85	662.83	92.87	850.25
Scenario 2	880.95	654.83	79.59	815.46
Scenario 3	864.17	629.13	79.49	789.57
Scenario 4	844.97	627.20	77.76	784.13

In Fig. 14, the probability distributions of energization overvoltages for the four scenarios are depicted, integrated with a normal distribution curve [31], [34]. Skewness and kurtosis are typically used to describe the variability of a data set. Skewness measures the degree of symmetry, or more accurately, the lack of it. Kurtosis evaluates whether the data have heavier or lighter tails compared to a normal distribution. Table 9 presents the skewness and kurtosis for the discussed scenario.

Across all scenarios, the mean skewness is positive, indicating that the probability distributions have longer tails on the right side compared to the left. Higher kurtosis values indicate that the probability distributions have sharper peaks than the normal distribution. Specifically, the peaks of the probability distributions in scenario 4 are sharper than other scenarios.

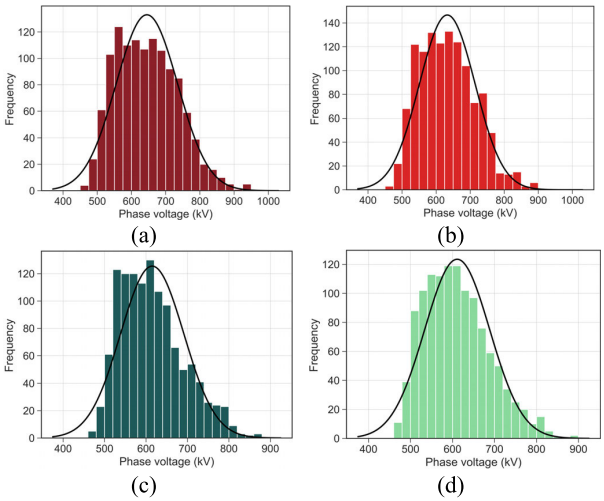

FIGURE 14. Probability of distribution of energization overvoltages (a) Scenario 1 (b) Scenario 2 (c) Scenario 3 (d) Scenario 4.

TABLE 9. Skewness and kurtosis of distribution overvoltages for line operating configuration case.

Scenario	Skewness	Kurtosis
Scenario 1	0.410	2.690
Scenario 2	0.409	2.725
Scenario 3	0.627	2.882
Scenario 4	0.597	3.002

2) IMPACT VARIATION OF SHORT-CIRCUIT POWER

The variations in short-circuit power at the Paiton substation are illustrated in Table 10. In this simulation, the utilized network topology was aligned with scenario 1 from the previous study, in which only a single circuit was operational on the Paiton–Kalipuro line.

TABLE 10. Short-circuit power variation at paiton substation.

Scenario	Parameters			
	Short-Circuit Power (MVA)	R/X	X_0/X_1	R_0/X_0
Scenario 1	12727	0.057	0.324	0.018
Scenario 2	11262	0.059	0.326	0.020
Scenario 3	8788	0.066	0.312	0.025

From Fig. 15, it can be seen that scenario 1, characterized by the highest short-circuit power, results in the highest overvoltage. The probability distributions of energization overvoltages for the three scenarios are depicted in Fig. 16. Table 11 shows the skewness and kurtosis for scenarios with varying short circuit power. As the short-circuit power decreases, the skewness also decreases correspondingly, indicating that the data set approaches symmetry similar to a normal distribution curve. The same trend applies to kurtosis, indicating that the probability distribution values become increasingly smaller than those of a normal distribution as the short-circuit power decreases.

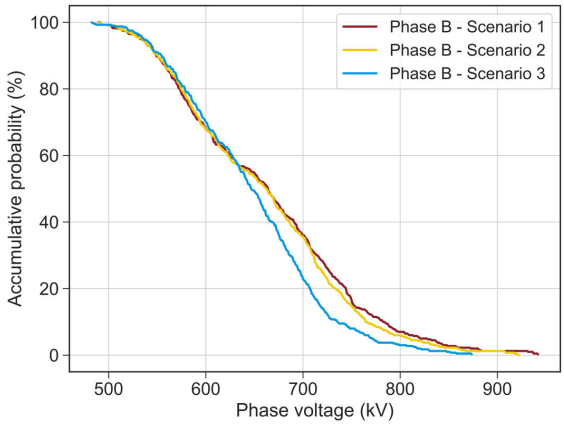

FIGURE 15. Accumulative probability distribution of overvoltages for variation of short-circuit power.

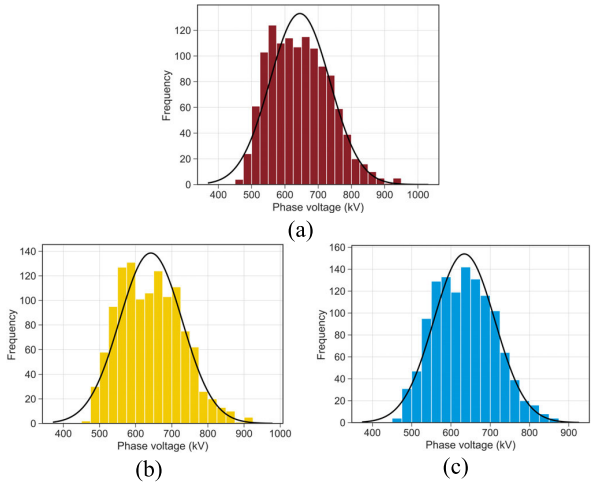

FIGURE 16. Probability of distribution of energization overvoltages (a) Scenario 1 (b) Scenario 2 (c) Scenario 3.

TABLE 11. Skewness and kurtosis of distribution overvoltages for variation of short-circuit power.

Scenario	Skewness	Kurtosis
Scenario 1	0.410	2.690
Scenario 2	0.369	2.623
Scenario 3	0.267	2.613

V. LINE DE-ENERGIZATION IN HYBRID OHL-SUBMARINE CABLE

When a CB is opened to de-energize a circuit, transient phenomena are also initiated. Re-ignition or restrike happens when the TRV exceeds the dielectric breakdown voltage between the contacts of the CB. A breakdown after the current interruption occurring within a quarter of a power-frequency

cycle (i.e., 5 ms in a 50 Hz system) is characterized as re-ignition, whereas restrike is a breakdown occurring later [11].

The approach adopted by the IEC involves defining envelopes of TRVs in the voltage–time plane. For each short-circuit test duty, TRV parameters are delineated as a function of the rated voltage U_r and the first-pole-to-clear factor. According to IEC 62271-100 [35], in cases where the TRV exhibits a multi-frequency nature, particularly at rated voltages of 100 kV and above, a four-parameter TRV is specified, which is illustrated in Fig. 17.

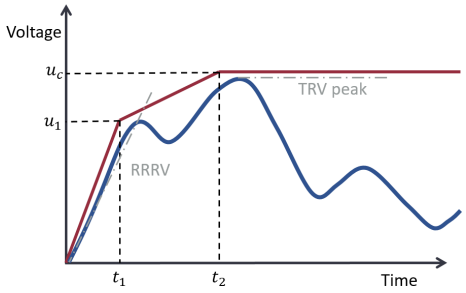

FIGURE 17. Standard IEC TRV envelope.

For analyzing transient voltages after the de-energization of circuit 2 of the JBC project, while circuit 1 is assumed to be out of service, two scenarios are presented. The first is the disconnection of both the circuit (SR remain connected), and the second is the disconnection of the circuit due to a terminal fault. For all simulations, at t = 100 ms (scenario 1) and at t = 90 ms (scenario 2), the open command was given to the breakers at both sides, and the breakers were assumed to interrupt the current at the first current zero crossing.

A. DISCONNECTION OF BOTH CIRCUIT AND SR

In Fig. 18, the TRV across the contacts of CB03-B after the de-energization process are depicted.

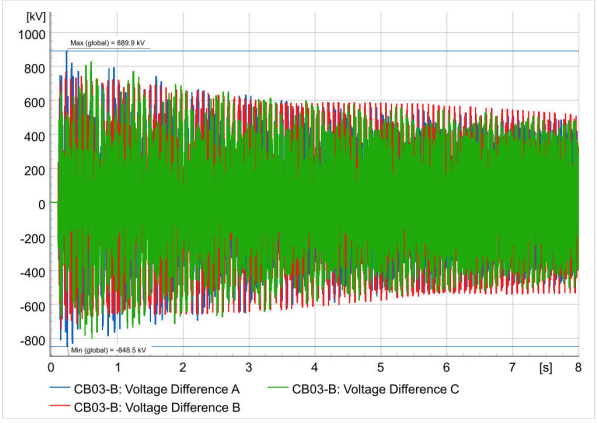

FIGURE 18. Voltage at kalipuro substation after de-energizing process.

The highest amplitude of the recovery voltage is observed in phase A, approximately 890 kV (2.18 pu). This is due to the higher initial voltage of this phase compared to the other phases in the disconnected circuit. The natural frequency is 38 Hz for reactor compensation degree of around 49%. In Fig. 19, the voltage at the OHL sending node (Kalipuro side) is depicted after de-energization while the SR is still connected. After a few seconds, all phase voltages drop to almost zero, with each phase experiencing a different voltage transition pattern.

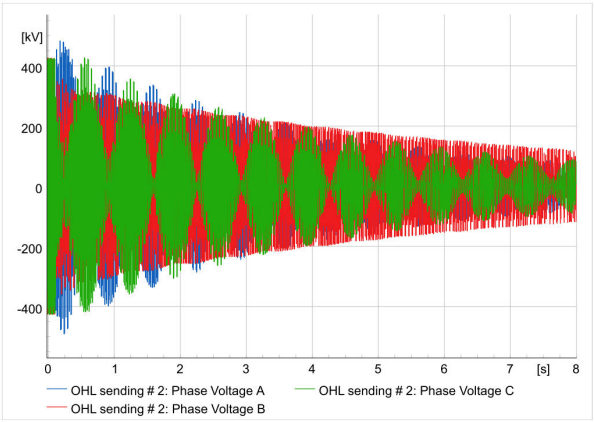

FIGURE 19. Voltage at OHL sending (Kalipuro side).

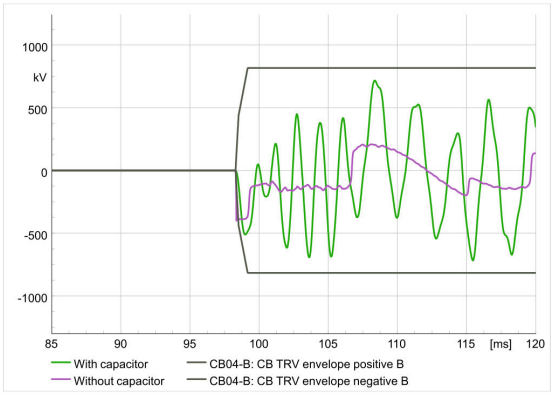

FIGURE 20. TRV at CB04-B at antosari side.

B. SHORT-CIRCUIT CURRENT INTERRUPTION

A three-phase short-circuit occurs at the terminal of CB04-B (i.e., the CB on the Antosari substation side) at t = 0 s while circuit 1 of Kalipuro-Antosari is deactivated. Subsequently, the CB at the Kalipuro substation and Antosari are simultaneously opened at 90 ms. Fig. 20 illustrates the TRV at CB04-B and the limiting line segment (envelope with test duty T100). It appears that the very high RRRV passes through the segment, while the first peak voltage remains relatively low. Adding capacitance will reduce the steepness of the RRRV but will result in an increased first peak voltage. The addition of capacitance decreases damping, which causes the amplitude of the voltage to rise and the voltage to become more oscillatory.

VI. CONCLUSION

The switching process generates transients. In EHV systems, transient overvoltages due to switching are more critical than those caused by lightning. Transients are described in terms of electromagnetic fields and traveling waves. Due to structural differences, hybrid OHL-submarine cable systems will experience complex transmission and reflection of electromagnetic waves, particularly at junction, leading to overvoltages that reach maximum values at the receiving end. Temporary overvoltage caused by parallel resonance will not occur in the JBC case when the SR is energized because the degree of SR compensation is only 49%.

Statistical distributions with 400 simulations of energization are produced by varying the circuit configuration and the system short-circuit power. The SWV during the energization process is found to remain below the specified 1175 kV. Moreover, it is concluded that transient energization overvoltages are likely to be higher when there is an increase in the network's short-circuit power. The probability distribution is fitted to a normal distribution, with the skewness and kurtosis shown to be skewed to the right and having a lower peak than that of the normal distribution, respectively.

When the SR remains connected to the phases as a hybrid OHL-submarine cable circuit is turned off, decaying oscillatory AC voltages with superimposed frequencies are exhibited by the disconnected phases. RRRV and TRV peak characterize the TRV. TRV due to a fault is more severe than that due to normal switching. Simulations show that when a three-phase short-circuit at the line breaker is induced, the RRRV exceeds the IEC standard envelope if only one circuit is operating.

REFERENCES

[1] *IEC Standard Voltages*, Standard IEC 60038, 2023.

[2] *Rencana Usaha Penyediaan Tenaga Listik PT. PLN (Persero)*, Ministry Energy Mineral Resour. Republic Indonesia, Jakarta Pusat, Indonesia, 2021.

[3] T. Worzyk, *Submarine Power Cables—Design, Installation, Repair, Environmental Aspects*. Springer, 2009.

[4] Z. Liu, J. Hao, R. Liao, J. Li, Z. Gao, and Z. Liang, "Morphological, structural, and dielectric properties of thermally aged AC 500 kV XLPE submarine cable insulation material and its deterioration condition assessment," *IEEE Access*, vol. 7, pp. 165065–165075, 2019.

[5] L. Zhao et al., "Research on transient overvoltage of transmission lines combined with 500 kV XLPE submarine cable and overhead line," in *Proc. 8th Renew. Power Gener. Conf. (RPG)*, Oct. 2019, pp. 1–5.

[6] X. Du, X. Liu, Y. Tang, T. Li, S. Wang, and N. Li, "Research on the optimization of grounding methods and power loss reduction based on AC 500kV XLPE submarine cable project," in *Proc. IEEE Int. Conf. Properties Appl. Dielectric Mater.*, Johor Bahru, Malaysia, Jul. 2021, pp. 394–397.

[7] Z. Zhi-Peng, L. Ying, L. Zhen-Qiang, and W. Lei, "Analysis of overvoltage and insulation coordination on 500kV AC cable transmission line," in *Proc. 8th Asia Conf. Power Electr. Eng. (ACPEE)*, Apr. 2023, pp. 2222–2227.

[8] DIgSILENT GmbH. (2022). *DIgSILENT PowerFactory User Manual*.

[9] *Insulation Co-ordination—Part 4: Computational Guide to Insulation Co-ordination and Modelling of Electrical Networks*, Standard IEC 60071-4:2004, 2004.

[10] S. Subedi et al., "Review of methods to accelerate electromagnetic transient simulation of power systems," *IEEE Access*, vol. 9, pp. 89714–89731, 2021.

[11] R. Smeets, L. van der Sluis, M. Kapetanovic, D. F. Peelo, and A. Janssen, *Switching in Electrical Transmission and Distribution Systems*. Hoboken, NJ, USA: Wiley, 2015.

[12] L. van der Sluis, *Transients in Power System*. Hoboken, NJ, USA: Wiley, 2021.

[13] *Power System Technical Performance Issues Related to the Application of Long HVAC Cables*, document C4.502, CIGRE Work. Group, 2013.

[14] H. Xue, J. Mahseredjian, J. Morales, I. Kocar, and A. Xemard, "An investigation of electromagnetic transients for a mixed transmission system with overhead lines and buried cables," *IEEE Trans. Power Del.*, vol. 37, no. 6, pp. 4582–4592, Dec. 2022.

[15] T. Gonen, *Electrical Power Transmission System Engineering Analysis and Design*. Boca Raton, FL, USA: CRC Press, 2014.

[16] M. H. Samimi, I. Ahmadi-Joneidi, A. Majzoobi, and S. Golshannavaz, "Appropriate selection of shunt compensation reactor in parallel transmission lines: A case study," *Int. J. Electr. Power Energy Syst.*, vol. 96, pp. 163–173, Mar. 2018.

[17] M. V. Escudero and M. Redfern, "Parametric analysis of parallel resonance on shunt compensated transmission lines," in *Proc. Int. Universities Power Eng. Conf.*, 2004, pp. 1–18.

[18] R. Smeets, S. Kuivenhoven, and A. B. Hofstee, "Realization of transient recovery voltages for ultra high voltage circuit breakers in testing," in *Proc. Int. Conf. Power Syst. Transients*, Del, 2011, pp. 1–16.

[19] *Konduktor Aluminium Berinti Baja Lapis Aluminium (A1/SA1A) Untuk Saluran Udara Tegangan Tinggi Dan Ekstra Tinggi*, document SPLN T3.001-1, 2015.

[20] *Guidelines for Representation of Network Elements When Calculating Transients*, document C WG33, 1990.

[21] *Rencana Penyediaan Tanaga Listrik Sistem Jawa Madura Bali Periode 2023–2027*, document 01/RK/P2B-REN-RNS/2022, Dec. 2022.

[22] T. Keokhoungning, S. Premrudeepreechacharn, and K. Ngamsanroaj, "Evaluation of switching overvoltage in 500 kV transmission line interconnection nam theun 2 power plant to Roi Et 2 substation," in *Proc. Asia–Pacific Power Energy Eng. Conf.*, Mar. 2009, pp. 1–28.

[23] K. Ngamsanroaj and W. Tayati, "An analysis of switching overvoltages in the EGAT 500 kV transmission system," in *Proc. Large Eng. Syst. Conf. Power Eng.*, 2003, pp. 149–153.

[24] DIgSILENT GmbH. (2022). *DIgSILENT PowerFactory Technical Reference External Grid ElmXnet*.

[25] H. Khalilnezhad, "Technical performance of EHV power transmission systems with long underground cables," M.S. thesis, Dept. Elect. Eng., Delft Univ. Technol., Delft, The Netherlands, 2018.

[26] PT. PLN (Persero) Divisi Perencanaan dan Enjiniring Konstruksi. (2021). *Dokumen Studi Kelayakan Java–Bali Connection (JBC)*.

[27] *IEEE Guide for Bonding Shields and Sheaths of Single-Conductor Power Cables Rated 5 KV Through 500 KV*, IEEE Standard IEEE Std 575TM-2014, 2014.

[28] DIgSILENT GmbH. (2022). *DIgSILENT PowerFactory Technical Reference Cable System*.

[29] *Kriteria Disain Tower Rangka Baja (Latticed Steel Tower) Untuk Saluran Udara Tegangan Tinggi Dan Saluran Udara Tegangan Ekstra Tinggi*, document SPLN T5.004:2010, 2010.

[30] *Standardisasi Spesifikasi Teknis Material Transmisi Utama (MTU) Dan Penjelasannya*, document SK DIR, no. 216.K/DIR/2013, 2013.

[31] T. Ohno, C. L. Bak, A. Ametani, W. Wiechowski, and T. K. Sørensen, "Statistical distribution of energization overvoltages of EHV cables," *IEEE Trans. Power Del.*, vol. 28, no. 3, pp. 1423–1432, Jul. 2013.

[32] A. I. Ibrahim and H. W. Dommel, "A knowledge base for switching surge transients," in *Proc. Int. Conf. Power Syst. Transients*, 2005, pp. 1–18.

[33] C. Yu, N. Petcharaks, and C. Panprommin, "The statistical calculation of energization overvoltages, case of EGAT 500 kV lines," in *IEEE Power Eng. Soc. Winter Meeting. Conf. Proc.*, Aug. 2000, pp. 2705–2709.

[34] H. Khalilnezhad, M. Popov, L. van der Sluis, J. A. Bos, and A. Ametani, "Statistical analysis of energization overvoltages in EHV hybrid OHL–Cable systems," *IEEE Trans. Power Del.*, vol. 33, no. 6, pp. 2765–2775, Dec. 2018.

[35] *High-voltage Switchgear and Controlgear—Part 100: Alternating-current Circuit-breakers*, Standard IEC 62271-100, 2021.